A MODEL BASED APPROACH TO IMPROVE THE PERFORMANCE OF THE GEOMETRIC FILTERING SPECKLE REDUCTION ALGORITHM

L. J. Busse, T. R. Crimmins*, and J. R. Fienup**

TETRAD Corporation, Englewood, Co. 80112
*MATHCOR Inc., Ann Arbor, MI 48105
**Environmental Research Institute of Michigan, Ann Arbor, MI 48113

ABSTRACT

This paper presents the methods used to adapt the geometric filtering method for speckle reduction to ultrasound imaging. The geometric filtering method is an iterative algorithm for speckle reduction which was first applied to radar images obtained with well controlled axial and lateral resolution. The appearance of speckle in ultrasound images is directly related to the size of the point-spread-function which is known to vary through-out a single frame. In order to optimally apply the speckle reduction algorithm in ultrasound, the effects of transducer geometry, center frequency shifts, and beamforming geometry were modeled and used to resample either the raw or video data before speckle processing. As a result of this approach, less data needs to be processed and the number of iterations are reduced. Using commercially available signal processing hardware, speckle reduced ultrasound frames can be processed and displayed at rates approaching 2 per second. This improvement in throughput facilitates the clinical evaluation of the geometric filtering method for improving lesion detection and overall image interpretability.

Introduction

The overall motivation for this work is to develop methods which can be used to reduce the speckle noise in ultrasound images. Speckle noise is the primary factor which limits the contrast resolution in diagnostic ultrasound imaging, thereby limiting the detectability of small, low contrast lesions and making ultrasound images generally difficult for the non-specialist to interpret. Speckle noise also limits the effective application of automated computer analysis (e.g., edge detection) and display (e.g., volume rendering and 3D display) algorithms. This paper describes how a specific speckle reduction algorithm known as the geometric filter (GF) has been adapted to the special requirements imposed by ultrasound imaging.

The geometric filter is a nonlinear, iterative algorithm which reduces speckle noise in images. It derives its name from the fact that it is based upon geometric concepts (convex, 8-Hull) first described in a paper by Crimmins[1] using both binary images and synthetic aperture radar images. The algorithm was described in greater detail in later publications by Crimmins[2,3] and demonstrated using radar imagery, GF was shown to effectively reduce speckle noise while preserving important image details. GF was later applied to ultrasound images[4] of contrast resolution phantoms and it was demonstrated that the contrast-to-speckle ratio (defined below) could double for low contrast lesions following three iterations of GF on a single ultrasound frame.

GF was subsequently applied to images of many anatomical features obtained with different styles of arrays. It was immediately noted, that the effectiveness of the filter was determined by the "field of view" (FOV) or the effective spatial sampling rate of the image. Images recorded with a small FOV (i.e., high spatial sampling rate) required many iterations of the GF to produce acceptable results while images recorded with a large FOV (i.e., low spatial sampling rate) sometimes appeared to be over-smoothed following only one iteration of the GF. The specific goal of this work is to link the spatial sampling rate to the actual spatial resolution in the ultrasound data so that the GF can be optimally, and uniformly applied. A model of the lateral and axial resolution as a function of transducer geometry, center frequency, and RF-processor was developed and used to determine raw and video data resampling rates which are applied before application of the GF. By following this approach, effective speckle reduction can be achieved with only a single iteration of the GF.

Theory

The optimum filter performance of GF is achieved when the speckled imagery is sampled at two points per resolution cell[2]. Because of the non-uniform nature of spatial resolution in ultrasound imaging, models were developed which could be used to guide or control the resampling of ultrasound imagery. The models used the following parameters:

z	Range
z_m	Range of the mth row in an image
α	Attenuation coefficient
f_o	Initial Pulse Center Frequency
$\varphi(z)$	Effective Pulse center frequency
$\lambda(z)$	Effective wavelength as a function of range (z)
p_l	Lateral pixel dimension
p_a	Axial pixel dimension
w	Receive aperture width

The model was developed for a specific ultrasound imaging system (TETRAD E/U 2200) and a variety of probe model geometries to include the effects of: 1) attenuation on pulse center frequency and wavelength, 2) cutoff frequency of RF-high pass filter in the RF processor, and 3) dynamically expanding receive aperture.

Pre-print of paper PK-1, presented Nov. 9, 1995
IEEE Ultrasonics Symposium, Seattle, Washington.

Pulse center frequency and attenuation: An idealized pulse with a gaussian power spectrum with 60% fractional bandwidth was used. The attenuation was then included using an exponential attenuation coefficient of -0.00576 nepers/(mm-MHz) which corresponds to the typical value of 0.5 dB/(cm-MHz). These assumptions lead to the following expression for pulse power spectrum as a function of depth:

$$g(f,z) = \exp\left\{-\left[f-\left(f_0 - 0.0007476 f_0^2 z\right)\right]^2 / \left(0.0649 f_0^2\right)\right\} \quad [1]$$

The effect of attenuation is to shift the center frequency of the pulse spectrum down as the range increases. To compensate for this effect, most ultrasound systems include some sort of high pass filter in the signal processing path. The E/U 2200 includes a 5-pole Bessel high-pass filter with selectable cutoff frequency *fc* with the transfer function:

$$H(f') = \frac{f'^5}{f'^5 + i2.42741 f'^4 - 2.61881 f'^3 - i1.58923 f'^2 + 0.55110 f' + i0.08918} \quad [2]$$

where $f' = f/fc$. Therefore the power spectrum of the filtered attenuated signal is $g(f,z)\left|H(f/fc)\right|^2$ for $f \geq 0$, depth z, and cutoff frequency *fc*. The effective center frequency, $\varphi(z)$, of the filtered attenuated signal is the centroid of this function, i.e.,

$$\varphi(z) = \frac{\int_0^\infty f g(f,z)\left|H\left(\frac{f}{fc}\right)\right|^2 df}{\int_0^\infty g(f,z)\left|H\left(\frac{f}{fc}\right)\right|^2 df}. \quad [3]$$

Lateral Resolution: The lateral resolution of a diffraction limited ultrasound imaging system is directly proportional to the effective wavelength and the F_{number} (or *w/z*). The system modeled uses a dynamically expanding receive aperture and attempts to maintain a constant receive F_{number} of 2 for all depths until it can no longer increase the width of the receive aperture. The expression for lateral resolution r_l can therefore be written:

$$r_l(z) = K_1 * \lambda * Fnumber = \frac{K_1 v \max(2w, z)}{w\varphi(z)} \quad [4]$$

where K_1 is a proportionality constant which depends upon details of aperture shape and apodization. The lateral resolutions can also be expressed relative to the lateral pixel dimension p_l.

$$\frac{r_l(z)}{p_l} = \frac{K_1 v \max(2w, z)}{p_l w\varphi(z)} \equiv K_1 r_l'(z) \quad [5]$$

where $r_l'(z)$ is then defined by this expression as the theoretical relative horizontal sample rate.

The experimental relative horizontal sampling rate was estimated by making images of phantoms containing fully developed speckle patterns and then performing an autocorrelation analysis. The experimental horizontal relative sampling rate $r''_l(z)$ can be shown[5] to be proportional to the half-width of the "horizontal autocorrelation" function. The proportionality constant K_1 is then chosen so as to minimize $\sum_{m=1}^{M}[K_1 \cdot r_l'(z_m) - r_l''(z_m)]^2$ where z_m now represents the range associated with the m^{th} row in an image.

Axial Resolution: In ultrasound imaging, axial resolution is directly proportional to the pulse length or the minimum resolvable time interval for a pulse with a given bandwidth and effective wavelength $\lambda(z)$. In pulse-echo imaging, the axial resolution is half the pulse width. If the pulse contains K_2 wavelengths, then the axial resolution is:

$$r_a(z) = K_2\lambda/2 = \frac{K_2 v}{2\varphi(z)} \quad [6]$$

The parameter K_2 will actually depend on details of pulse shape and bandwidth and is to be determined by fitting experimental data. The axial resolution can also be expressed relative to the axial pixel dimension p_a.

$$\frac{r_a(z)}{p_a} = \frac{K_2 v}{2p_a\varphi(z)} = K_2 r_a'(z). \quad [7]$$

where $r_a'(z)$ is defined as the theoretical relative axial sample rate. Again, using images of phantoms containing fully developed speckle and autocorrelation analysis, the experimental axial relative sampling rate $r_a''(z)$ can be "measured" and the proportionality constant is then determined as the value which minimized the expression $\sum_{m=1}^{M}[K_2 \cdot r_a'(z_m) - r_a''(z_m)]^2$.

Methods

The models described above were implemented using Matlab[6] and a database was included which contains 6 different probe models each with three different FOVs. Each combination of probe model and FOV was considered as a separate case since probe model effects physical parameters like pitch, frequency, etc. and FOV effects electronic parameters such as filter settings, video sampling rates, line-sampleing rates, etc. Image data of speckle patterns were recorded for each case and data used for the analysis were taken from the raw data memory (detected, compressed data prior to scan conversion) of the E/U 2200 imager.

The effectiveness of the GF process was quantified using two different measures of speckle noise: 1) the speckle index and 2) the contrast-to-speckle ratio.

The speckle index is related to the ratio of the local deviation in pixel brightness to the mean pixel brightness averaged over the entire image. Let f(m,n) represent our original image for $1 \leq m \leq M$ and $1 \leq n \leq N$. The local deviation is then defined as

$$\sigma(m,n) = \max_{-1\leq a,b\leq 1}(f(m+a,n+b)) - \min_{-1\leq a,b\leq 1}(f(m+a,n+b)) \quad [8]$$

and the local mean is defined as

$$\mu(m,n) = \frac{1}{9}\sum_{a,b=-1}^{1} f(m+a,n+b) \quad [9]$$

The speckle index *SI* is then defined as

$$SI \equiv \frac{1}{MN}\sum_{m=1}^{M}\sum_{n=1}^{N}\frac{\sigma(m,n)}{\mu(m,n)} \qquad [10]$$

Speckle index is an average measure of the amount of speckle present in the image as a whole.

Lesion detectability was quantified using the contrast-to-speckle ratio *CSR*[7]. The *CSR* is calculated by defining two regions of interest and using the mean pixel value and the pixel variance to quantify contrast $(\mu_1 - \mu_2)/\mu_1$, and speckle noise $(\sigma_1^2 + \sigma_2^2)^{1/2}/\mu_1$. The ratio of these two quantities is termed *CSR*:

$$CSR \equiv (\mu_1 - \mu_2)/(\sigma_1^2 + \sigma_2^2)^{1/2} \qquad [11]$$

CSR provides a quantitative measure of the detectability of low contrast lesions when one region is completely inside the lesion and the second is in the background media.

Results

Figure 1 shows an example of how the K_1 parameter was determined for a 6MHz, linear array imaging at the 100mm

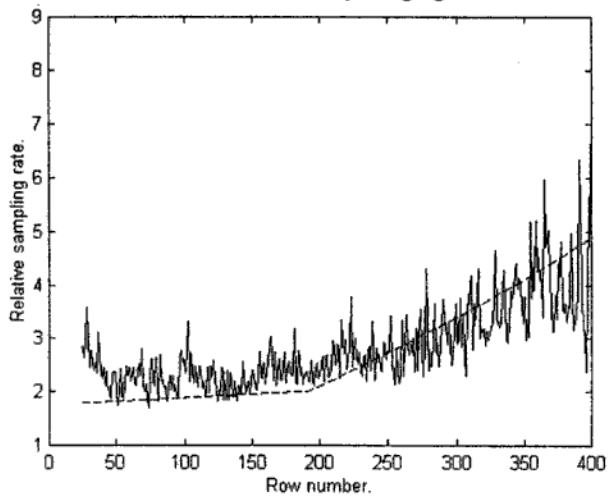

Figure 1. Experimental (solid) and Theoretical (dashed) lateral relative sampling rates. 6 MHz linear array, 100 mm FOV.

FOV. The jagged curve represents the experimental relative sampling rate obtained from the autocorrrelation analysis and the dashed line represents the best fit $(K_1 \cdot r_l'(z_m))$ to the data. The "low slope" region of the curve is in a region where the imaging system is able to maintain a constant receive F/number and the "high-slope" region is indicative of a fixed receive aperture size. Figure 2 shows an example of how the K_2 parameter was determined for the same array and field-of-view. The jagged line shows the relative vertical sampling rate obtained from the autocorrelation analysis and the dashed line shows the best fit $(K_2 \cdot r_a'(z_m))$.

Based on the relative sampling rates determined in this way, ultrasound images were resampled to bring both the lateral and axial relative sampling rates to 2 (i.e., two sample points per resolution cell) before speckle reduction processing was applied. This resampling could involve an arbitrary amount of interpolation and either up- or down- sampling. Following speckle reduction the inverse process was applied to

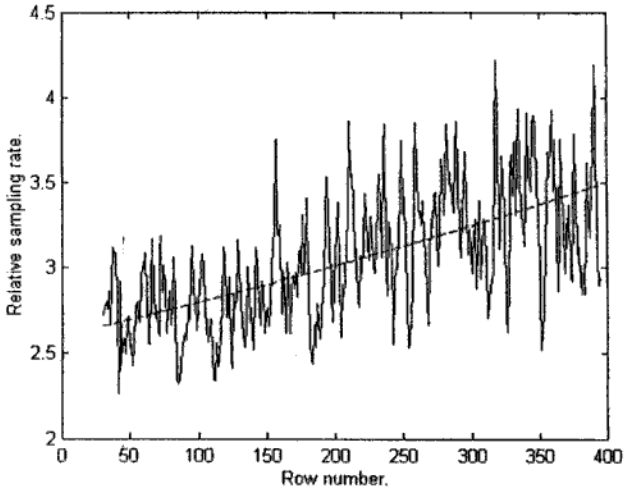

Figure 2. Experimental (solid) and Theoretical (dashed) axial relative sampling rates. 6 MHz linear array, 100 mm FOV.

return the images to their original sampling rates for scan-conversion and re-display. Figure 3 illustrates this resampling concept for the same linear array mentioned above. The axes of the graph show the original row and column numbers of the sampled data and the lines within the plot show where the uniform sample rate grid falls within the original grid. The plot shows the effect of constant F/number imaging in the near field, partial apertures near the edges of the image, and frequency down-shifting caused by exponential attenuation.

Ultimately, the computation necessary to put raw data onto the uniformly sampled grid USG was judged to be too time consuming and a more quantized version was implemented. The quantized form of the uniform sampling grid (QUSG) performed either up- or down-sampling by factors of 1.5, 2,3,4, etc., in an effort to keep the relative sampling rate as close as possible to 2. Using this strategy, the relative sampling rate was always maintained between 1.6 and 2.4. Since resampling was limited to integer values and 1.5, it

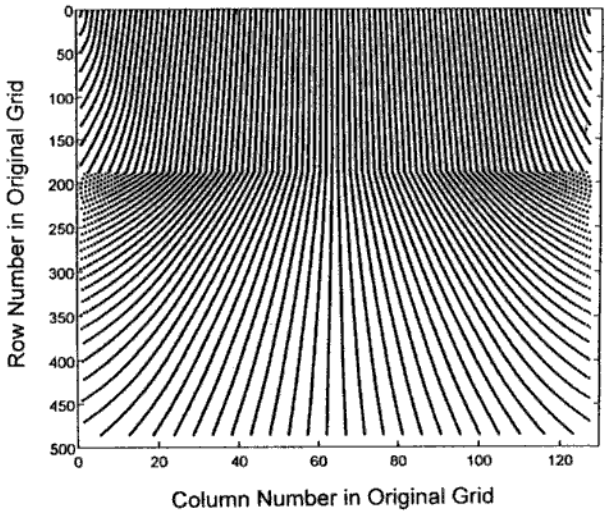

Figure 3. Uniform Sampling Grid placed within the Original data sampling grid. 6 MHz linear array, 100 mm FOV.

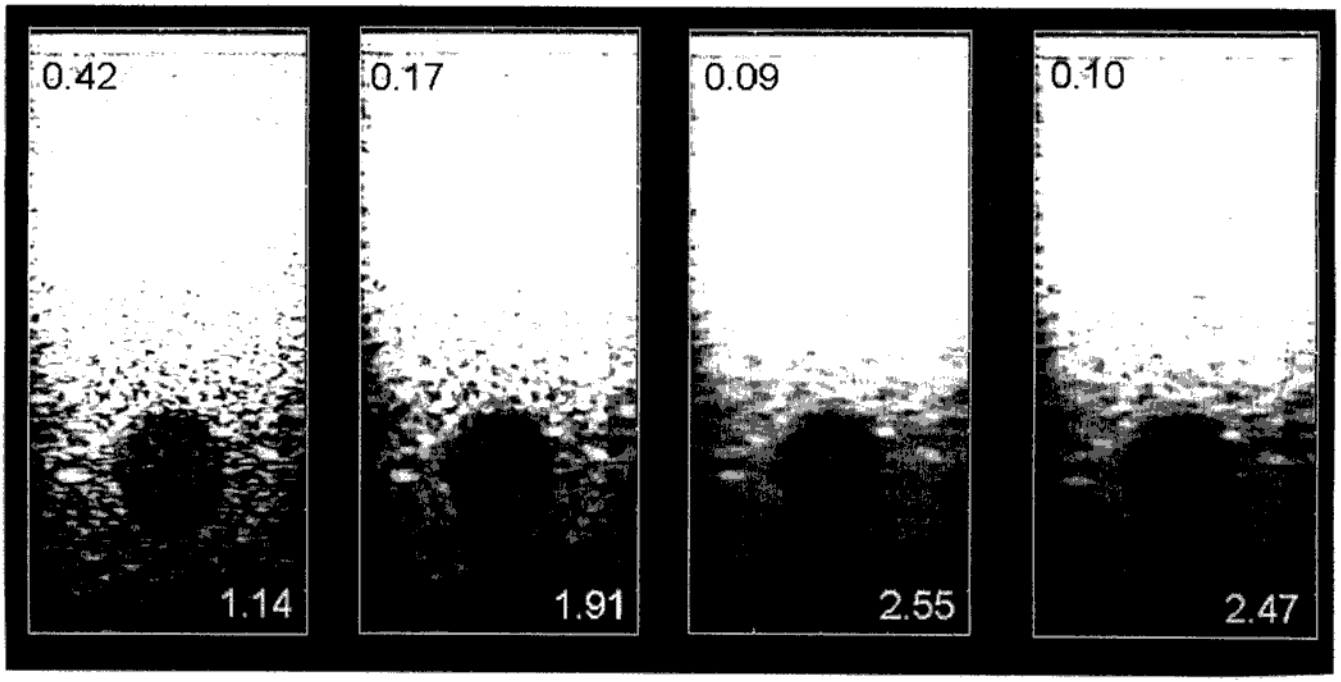

Figure 4. Images demonstrating the effect of spatial sampling rates upon the performance of the Geometric Filter. Panels (from left to right) show: 1) Original Image, 2) GF on original grid, 3) GF on USG, and 4) GF on QUSG. Object being imaged is a -8dB lesion inside a contrast resolution phantom.

could be implemented using faster decimation/interpolation routines.

Figure 4 shows examples of images processed in this way. From left to right these are images of 1) the original image before speckle reduction, 2) the same data following 2 iterations of the geometric filter on the original data grid, 3) the data processed using two iterations on the USG, and 4) the data following speckle reduction processing on the QUSG. Numbers in the upper left of the panels (black) are the speckle index for the image and the numbers in the lower right of each panel (white) are the CSR between the lesion and the adjacent background. The same degree of processing on either the USG or the QUSG has a greater effect than processing on the original grid. Images processed using the USG and QUSG were judged to be equivalent by human observers. Using the speckle index and contrast-to-speckle ratio to quantify the performance, only a slight penalty was noted by making use of the QUSG and computation time was significantly reduced. Using the quantitative indices of SI and CSR, the degree of speckle reduction achievable using one iteration of the filter on the USG or QUSG required 3 iterations of the same filter on the original grid. An additional benefit of using either the USG or QUSG is that the performance of the geometric filter is constant and independent of the model or field of view chosen.

Following the off-line processing and analysis of images, the core features of the algorithm were re-written in 'C' and assembly language to run on an Alacron[8] AL860 dual-processor system attached to a PC and frame-grabber. This system is currently able to capture live video from the ultrasound imaging system, resample, speckle-reduce and re-display the images at a rate of 2 frames per second. This processing rate, while not yet "real-time" is fast enough to allow for live scanning evaluations of the GF. The results of such scanning evaluations will be reported upon at a later date.

Acknowledgment

This work was supported by Grant CA-51581 from the National Cancer Institute. Its contents are solely the responsibility of the authors and do not necessarily represent the official views of the National Cancer Institute.

References

[1] T. R. Crimmins, "Geometric Filter for Speckle Reduction," *Applied Optics* 24(10) 1438-1443, 1985.

[2] T. R. Crimmins, "Geometric Filter for Reducing Speckle," *Optical Engineering* 25(5), 651-654, 1986.

[3] T. R. Crimmins, "A System for Reducing Speckle Noise", U.S. Patent 4,783,753 issued Nov. 8, 1988.

[4] L. J. Busse, D. R. Dietz, W. M. Glenn, Jr., "A Non-Linear Algorithm for Speckle Reduction," IEEE Ultrasonics Symposium 91CH3079-1, 1105-1108, 1991.

[5] Presentation of this theory is beyond the scope of this paper. Details can be found in CA51581 final report or in subsequent publications.

[6] MATLAB 4.0 by the MathWorks, 24 Prime PArk Way, Natick, MA, 01760.

[7] A. T. Kerr, M. S. Patterson, F. S. Foster, and J. W. Hunt, "Speckle Reduction in Oulse Echo Imaging using Phase Insensitive and Phase Sensitive Signal Processing," *Ultrasonic Imaging* 8, 11-28, 1986.

[8] Alacron Corporation, 71 Spitbrook Road, Nashua, NH, 03060.

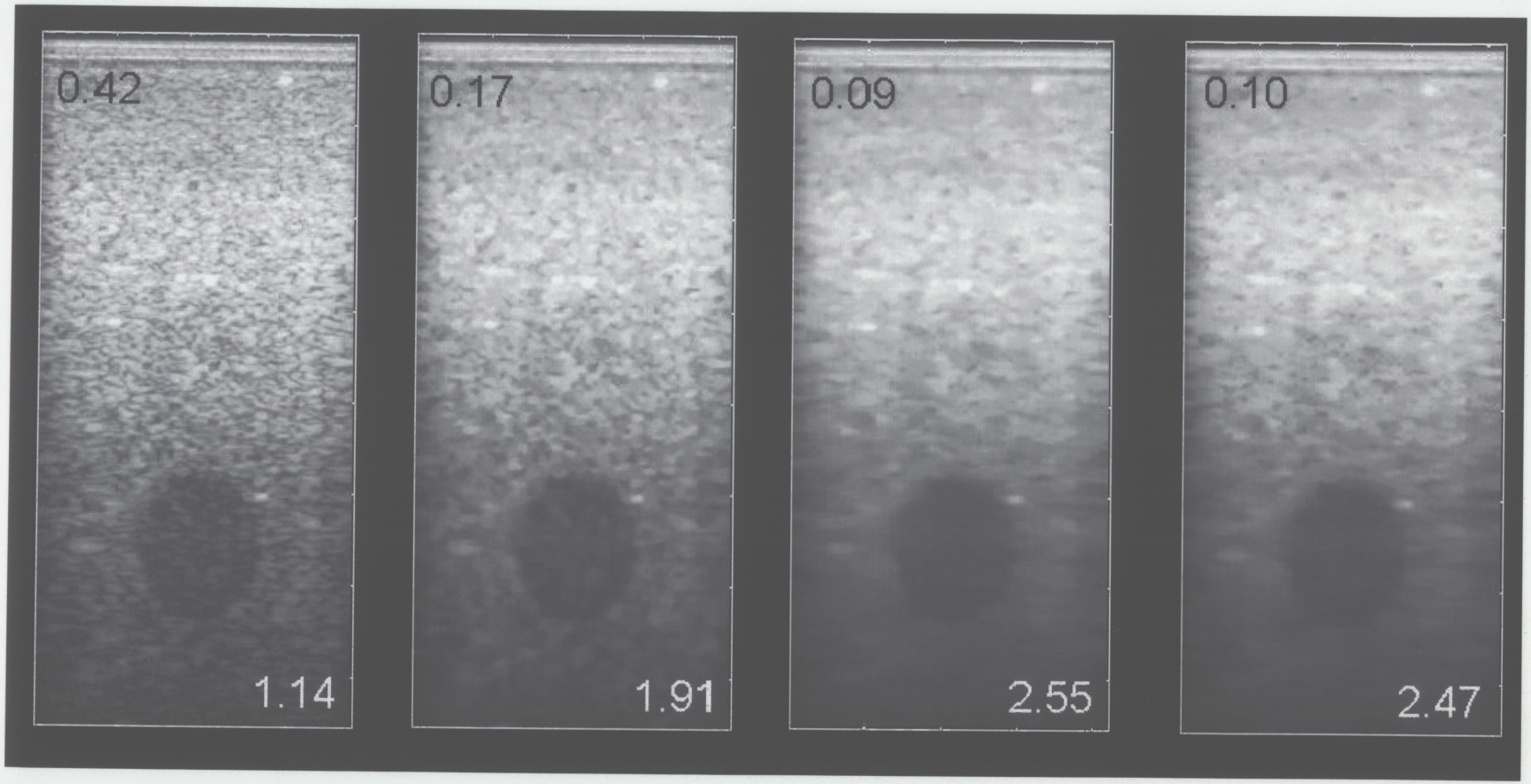
0.42
1.14
0.17
1.91
0.09
2.55
0.10
2.47